World Conference on Timber Engineering Oslo 2023

Experimental and Numerical Investigations on the Usage of CLT Panels to Form Timber-Steel Composite Floor Systems

Hugh Merryday[1], Megan Potuzak[2], David Roueche[3], Kadir Sener[4]

ABSTRACT: This paper presents experimental and numerical results from an ongoing investigation to evaluate the performance of steel-timber composite floor systems. A composite floor system comprised of cross-laminated timber (CLT) made from Southern Yellow Pine species was fastened to a hot-rolled wide flange steel beam using self-tapping wood screws. Experimental evaluations included pushout tests for mechanical fastener characterization and a beam test that was monotonically tested under a four-point bending setup. Beam test results were compared against a steel-timber fiber model, existing equations adapted from steel-concrete composite design, and experimental steel-CLT load-slip response from the pushout testing. Near full-composite behavior was observed in the beam prior to connection slip but reduced to partial-composite behavior as screws began to deform. A substantial increase in strength and stiffness was observed for the composite beam from the non-composite (hybrid) case which was nearly equal to the level of composite action achieved during the test. Both the section fiber model and adapted steel-concrete composite design equations estimated the steel-CLT beam behavior with reasonable accuracy compared to the experimental test.

KEYWORDS: Mass timber, steel-CLT composite beam, self-tapping screws

INTRODUCTION

The recent popularity of mass timber construction as an alternative to traditional materials such as steel, concrete and masonry can be credited to its designation as a renewable resource. Also, mass timber, such as cross-laminated timber (CLT), can improve construction times as modular elements are manufactured off-site and installed with minimal site work. However, due to limitations stemming from strength and serviceability, mass timber elements are not efficient for high-rise construction since deep glue-laminated beams are often required for large spans. Accordingly, Figure 1 depicts a popular design practice to address this challenge in which hybrid construction systems involve the use of mass timber floor panels as decking elements in steel-frame structures. Utilizing this system will enable smaller steel beams and girder sections while maintaining a CLT deck comparable to the more well-established steel-concrete construction. However, unlike steel-concrete construction, there is little to no guidance on the design of steel-timber composite construction. Thus, engineers must oversize steel members to work as floor members alone, ignoring any strength contribution provided by the CLT deck.

This paper presents ongoing experimental and numerical studies to evaluate the performance of steel-CLT composite beams using large diameter self-tapping screws as shear connectors. Previous experimental studies have been conducted on steel-CLT composite beams with the use of heavy-duty wood screws and bolted connections [1]; whereas in the US, self-tapping screws are a preferred choice in the mass-timber industry over other types of connection for their speed of installation (Figure 1). Static pushout tests have been conducted to evaluate the connection strength and to identify possible failure modes associated with three self-tapping screw types used in steel-timber composite construction [2]. This study also presents preliminary results from a large-scale beam test, informed by the pushout test results, conducted to investigate the flexural strength performance of steel-CLT composite using one of the self-tapping screw types. A section fiber model has been developed to predict the flexural behavior of steel-timber beams, accounting for partial composite action at the steel-timber interface. The model obtains both section-level and member-level behavior to provide a holistic summary of the beam's response. Finally, model results are compared with experimental data.

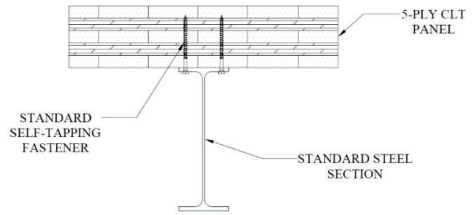

[1] Hugh Merryday, Auburn University, Department of Civil and Environmental Engineering, USA, hcm0044@auburn.edu
[2] Megan Potuzak, Auburn University, Department of Civil and Environmental Engineering, USA, mtp0027@auburn.edu
[3] David Roueche, Auburn University, Department of Civil and Environmental Engineering, USA, dbr0011@auburn.edu
[4] Kadir Sener, Auburn University, Department of Civil and Environmental Engineering, USA, sener@auburn.edu

https://doi.org/10.52202/069179-0439

Figure 1: *Typical cross-section of steel-CLT hybrid construction.*

2 METHODOLOGY

2.1 MATERIALS

CLT used in this study was manufactured from southern yellow pine at a nearby CLT production facility. According to manufacturer specifications, the alternating 5-ply layup consisted of visually graded No. 2 or better lumber in the outermost and middle layers and No. 3 or better in the remaining transverse layers in accordance with the National Design Specification (NDS) for Wood Construction [3]. The specific gravity and moisture content were measured in accordance with ASTM D2395 [4]. The moisture content was measured to be 10.2% and the specific gravity was measured to be 0.46±0.07 (mean and standard deviation) for 20 samples. Steel sections used for pushout and beam testing consisted of hot-rolled W16 x 31 (American designation) made from A992 steel with a measured yield strength of 385 MPa and ultimate strength 495 MPa as provided from the mill test report. Self-tapping screws used to attach CLT to steel are shown in Figure 2 and their geometric and material properties are shown in Table 1. The fastener bending yield strength, F_{yb}, was determined in accordance with ASTM F1575 [5]. In Table 1, L is the screw length, D_n is the nominal diameter, D_s is the shank diameter, and D_r is the root diameter.

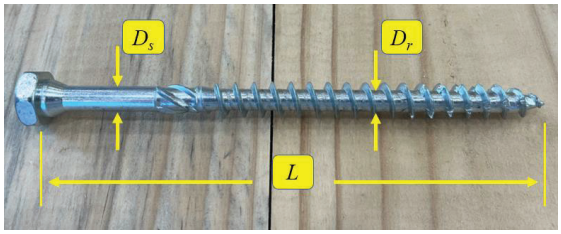

Figure 2: *Self-tapping screw used in beam test.*

Table 1: *Geometric and mechanical properties of self-tapping screws.*

L (mm)	D_n (mm)	D_s (mm)	D_r (mm)	F_{yb} (MPa)
160	12.7	8.1	6.9	1280

2.2 MONOTONIC PUSHOUT TESTS

Pushout tests were conducted using a symmetrical test setup, with two CLT panels fastened to each flange of the steel section with two rows of screws. CLT panels had dimensions of 457 mm wide by 610 mm tall with varying thickness depending on the number of laminations (35 mm per lamination). Steel sections measured 610 mm tall with adequate offset from the end of CLT panels to accommodate displacement. The standard test specimen is shown in Figure 3, with a typical layout of 8 screws. 12.7 mm holes were punched in the steel flange using a hydraulic punch to replicate field conditions. The transverse hole spacing was 102 mm leaving a 19 mm center-to-edge distance on the steel flange. To ensure screws were installed straight, a 6 mm pilot hole was provided, and the self-tapping screws were torqued to 54 N-m in accordance with manufacturers' recommended torque limits. Four potentiometers, one at each specimen corner, were used to measure the relative slip between the steel and CLT panels during testing. The load regime was adapted from ASTM D5652 [6], where load was applied under displacement control at a rate of 2.54 mm/min to reach the maximum load in approximately 10 minutes. Tests were stopped either when screw failure occurred, or 80 percent of the post-peak load was reached. Further details of the pushout tests are available in [2].

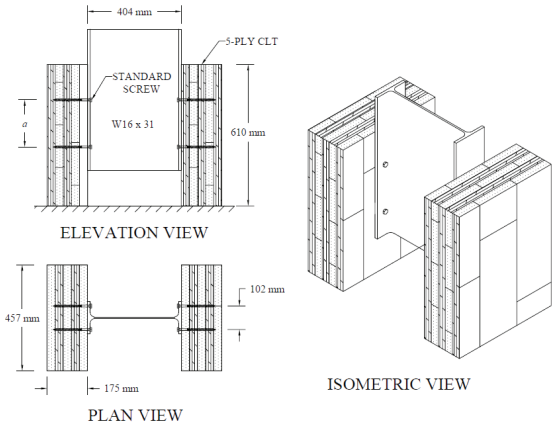

Figure 3: *Standard pushout test specimen.*

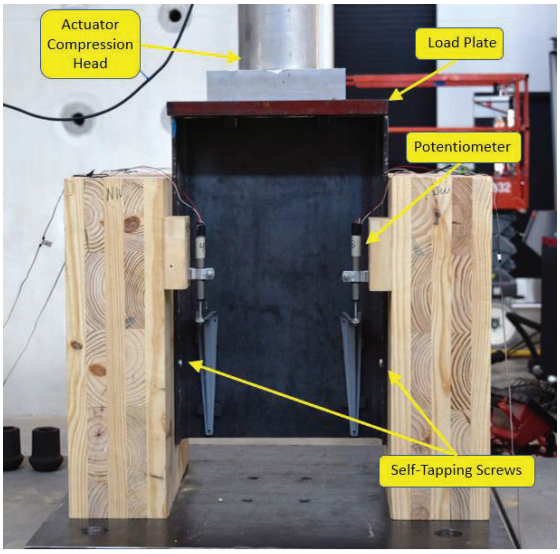

Figure 4: *Pushout test setup.*

2.3 LARGE-SCALE BEAM TEST

The beam test was conducted using a four-point bending test setup as shown in Figures 5 and 6, with a continuous 5-ply CLT panel fastened to a 9.14-meter long W16 x 31 steel member. The CLT deck measured 483 mm wide and was oriented so that the major strength direction was parallel to the length of the beam. Screws were installed at 305 mm spacing using methods outlined for pushout testing, without the use of pilot holes to mimic field application. Six string potentiometers were used to monitor and record vertical displacement at midspan, load points, and at the mid-shear spans. Four inclinometers were placed at mid-height of the steel section at each load point to measure rotation. Eight 25 mm slip sensors were used to measure the relative slip between the steel and CLT along the length of the beam. Strain gauges were attached to the steel and CLT within the constant moment region to capture the strain profile of the cross-section. Figure 7 illustrates the steel and wood strain gauge arrangement at midspan. Load was monotonically applied through a transfer beam under displacement control at a rate of 1.27 mm/min and was increased to 2.54 mm/min in the post-yield region. The test was stopped when the actuator stroke limit was reached. To limit out of plan deflection, Teflon plated bracing was provided at midspan with 3 mm of clearance as shown in Figure 8.

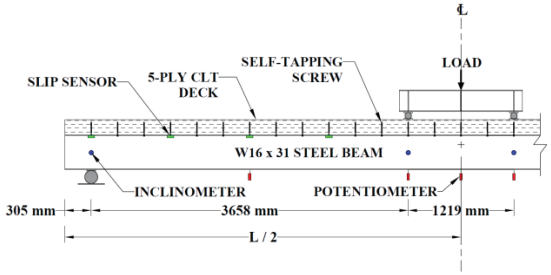

Figure 5: *Steel-CLT four-point bending test setup and instrumentation.*

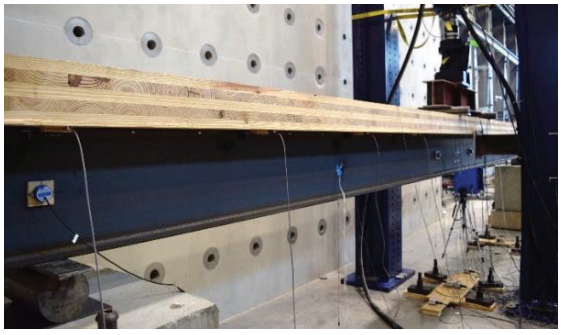

Figure 6: *Steel-CLT four-point bending test setup.*

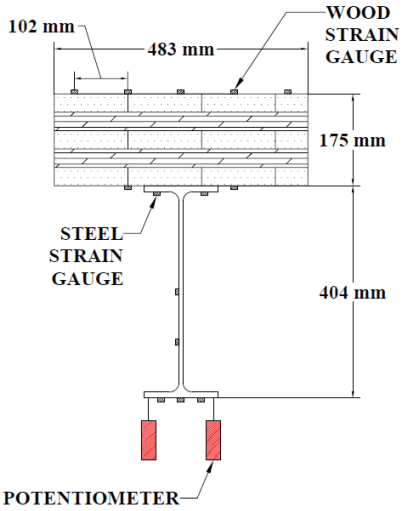

Figure 7: *Midspan instrumentation layout.*

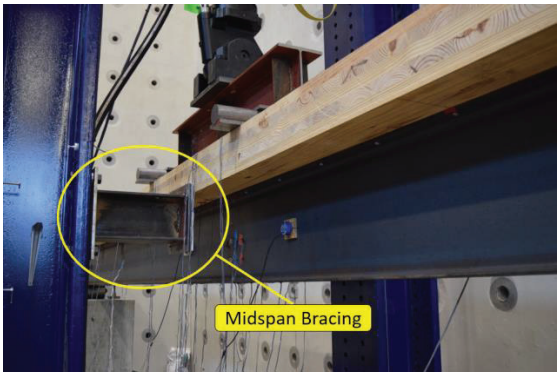

Figure 8: *Steel-CLT beam test specimen at midspan.*

2.4 NUMERICAL MODEL

A 2D section fiber model was developed to analyze the flexural behavior of steel-timber beams, accounting for the degree of partial composite action between the steel and timber, cross-sectional dimensions, mechanical properties, and timber orientation. The model discretizes the cross-section into small horizontal layers, which are assigned with uniaxial material properties and dimensions corresponding to each layer. In steel-CLT beams, different material properties were assigned to each layer of timber based on its orientation. Using fundamental constitutive relationships between stress and strain of each material and establishing force equilibrium, the cross-sectional stress and strain profiles were obtained at increasing curvatures. The percentage composite action incorporated into the strain calculation was obtained through calibration of slip strain measurement from testing, as provided in Equation (1).

$$CA_{strain} = (1 - \varepsilon_{slip\_test} \,/\, \varepsilon_{slip\_non-comp})\% \qquad (1)$$

https://doi.org/10.52202/069179-0439

In Equation (1), CA_{strain} = percentage composite action determined from slip strain, ε_{slip_test} = slip strain measured at curvature φ obtained from experimental test, and $\varepsilon_{slip\_non\text{-}comp}$ = slip strain under non-composite (0% composite) condition at curvature φ obtained from fiber model. The percentage composite action was assumed to be constant throughout the analysis that resulted in a linear relationship between slip strain and curvature.

The section moment was calculated for incrementally increasing curvature levels to develop the moment-curvature response of the cross-section, where equal curvature was assumed for steel and timber elements at the same cross-section. The numerical model steps to achieve the moment-curvature relationship are summarized in Figure 9. Once the moment-curvature relationship was obtained for the section, this response was integrated along the beam length to obtain member-level responses including mid-span deflection, interfacial slip at beam ends, and support rotation. The fiber analysis results were validated against a database of steel-timber beam tests, and the comparisons are discussed in detail elsewhere [7].

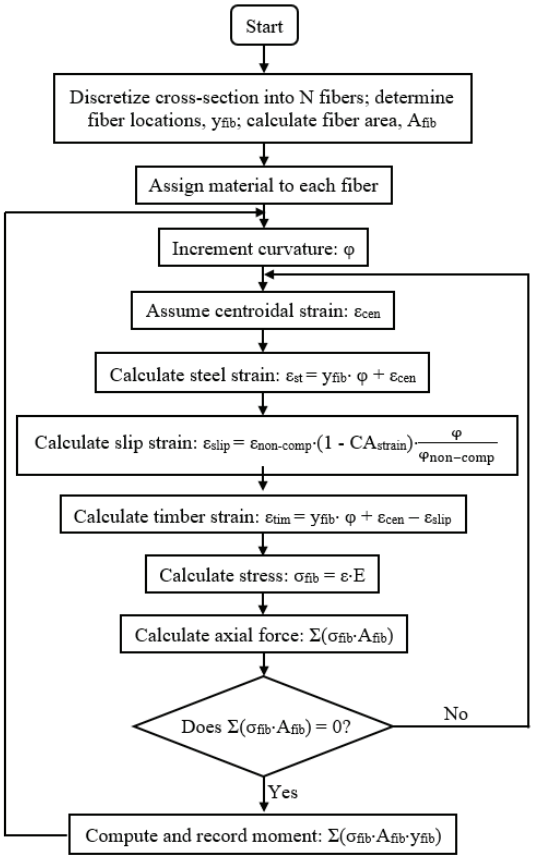

Figure 9: *Flowchart summarizing section fiber analysis model.*

2.5 STRENGTH AND STIFFNESS PREDICTIONS BASED ON AISC APPROACH

Since steel-concrete composite floors are a common structural system, extensive research has been performed to establish design equations to calculate beam stiffness and flexural capacity for these composite systems. Steel-timber composite flooring systems resemble steel-concrete composite systems in that they both pair low-tensile strength materials with structural steel members. Therefore, the applicability of typical steel-concrete composite design equations on steel-timber systems were evaluated. Understanding the correlation between these two structural systems as it pertains to partial composite action would accelerate the adoption of steel-timber composite structures into design provisions.

The design equations analyzed were adopted from the American Institute of Steel Construction (AISC) Specification [8]. The Specification provisions in Chapter I characterize composite action between structural steel members and concrete slabs as a fraction of the combined shear strength of the shear connectors within the shear span of the beam to the minimum strength contribution between the steel and concrete elements. Similarly, Equation (2) emulates the AISC steel-concrete composite system equation by replacing concrete compressive strength and shear stud strength with timber compressive strength and mechanical connector (self-tapping screw) shear strength:

$$CA_{strength} = \frac{\Sigma Q_n}{\min\left(A_s f_y, \Sigma f_{c,tim} A_{tim}\right)} \qquad (2)$$

where $CA_{strength}$ = percentage composite action based on strength, ΣQ_n = total shear strength of mechanical connectors located within the shear span, A_s = cross-sectional area of steel, f_y = steel yield strength, $f_{c,tim}$ = timber compressive yield strength, and A_{tim} = cross-sectional area of timber.

Once the partial composite action percentage is determined from Equation (2), the effective stiffness of each beam is calculated in accordance with the Specification Equation C-I3-3, as shown in Equation (3):

$$EI_{equiv} = E_s * [I_s + \sqrt{CA_{strength}}(I_{tr} - I_s)] \qquad (3)$$

where EI_{equiv} = equivalent flexural stiffness of steel-timber composite member, E_s = elastic modulus of steel, I_s = moment of inertia of steel, and I_{tr} = transformed moment of inertia of the steel-timber cross section.

Additionally, the plastic moment capacity was calculated for each steel-timber beam to compare the accuracy of experimental results, as outlined in Section I2a of the Specification. These calculations performed in accordance with the AISC Specification are compared to experimental data to draw conclusions about their applicability to steel-timber composite flooring systems.

https://doi.org/10.52202/069179-0439

3 EXPERIMENTAL RESULTS

3.1 PUSHOUT TESTS

Results of pushout testing for the screws used in this beam test have been previously presented in detail elsewhere, [2], but will be briefly summarized for the type of screw used in the beam testing.

Typical failure of the screws used for beam testing was associated with the formation of a single plastic hinge within the CLT accompanied by a brittle shear/tensile failure at the steel-CLT interface. The cross-section of a typical pushout test specimen with screws spaced at 203 mm is shown in Figure 10. This study concluded that the abrupt transition of the screw geometry between the head and shank disrupted the full development of a double plastic hinge. The representative load-slip response of the screws shown in Figure 11 demonstrated that the screws have an average strength of 29.8 kN/screw corresponding to an average maximum slip of 17.3 mm. The connection was also observed to experience a region of no slip due to torquing during initial parts of the loading, as highlighted in Figure 11.

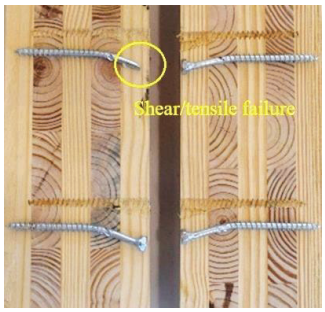

Figure 10: *Failure mode of self-tapping screws loaded parallel to outer lamination in steel-timber pushout setup.*

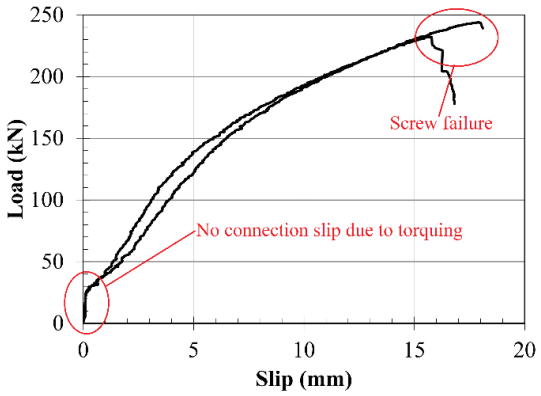

Figure 11: *Load-slip response of steel-CLT connection comprised of eight self-tapping screws.*

3.2 BEAM TEST

No distinct failure mode was observed as the test was stopped due to the constraints of the actuator stroke as shown in Figure 12. Though not a limiting factor for strength, Figure 13 depicts initiation of crushing of timber at a finger joint location on the top surface near midspan. It should also be noted that the beam experienced two instances of support settlement, where the roller/pin setup adjusted to accommodate large rotations.

The load vs. midspan displacement, load vs. support rotation, and load vs. average relative slip between the steel and CLT at the supports are presented in Figures 14, 15, and 16, respectively. The load vs. displacement plot indicated a stiff response until relative slip initiated at the steel-timber interface. The reduced stiffness response was linear until yielding initiated in the steel member at around 150 kN. The load gradually increased in a nonlinear fashion until the actuator stroke limit was achieved (250 mm), and the specimen was unloaded.

The load vs. rotation and load vs. slip plots were observed to follow a similar response to the load-displacement, where a reduced stiffness response was followed by a post-yield nonlinear response until stoppage. However, the load slip response depicts a region of no slip between the steel and CLT at the support up to a load of 25 kN when slip initiated. A linear slip response was observed until steel yielding, at which a nonlinear response occurred.

The relative slip between the steel and CLT along the beam corresponding to various load levels is shown in Figure 17. The slip is observed to increase with distance away from load points and indicated a nearly symmetric slip-response in each shear span. The section strain profiles at the initiation of yielding and at ultimate loading conditions is shown in Figure 18, indicating the shifting in each neutral axes observed in CLT and steel with nearly identical curvature in both members. The variation in wood strains across the width of the CLT top surface is shown in Figure 19. The compressive strains in the wood members were observed to be uniform until nearing the ultimate load, where one side experienced more strain.

The service-level stiffness (EI_{eff}), support rotation, and beam end slip corresponding to the ultimate load are provided in Table 2. The service-level stiffness was calculated as the tangent slope of moment-curvature responses between moments corresponding to 80 and 120 kN-m. The yield and ultimate displacements are provided in Table 3, where yielding is defined as the initiation of yielding based on steel tension strain measurements.

https://doi.org/10.52202/069179-0439

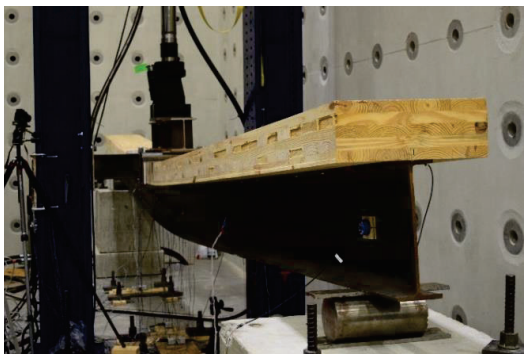

Figure 12: *Beam at ultimate loading condition.*

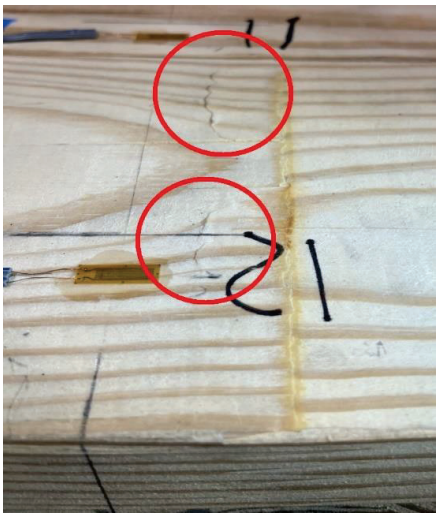

Figure 13: *Crushing of timber lamination at midspan finger joint location.*

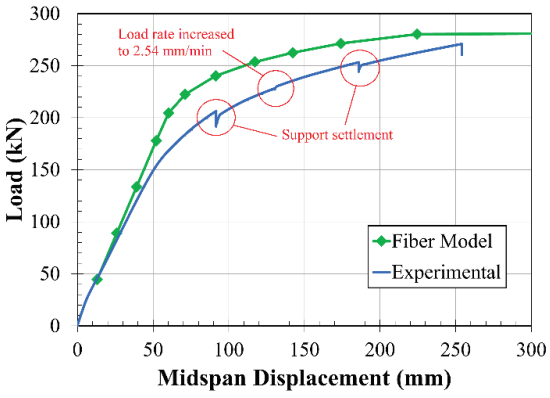

Figure 14: *Experimental midspan displacement compared with fiber analysis results.*

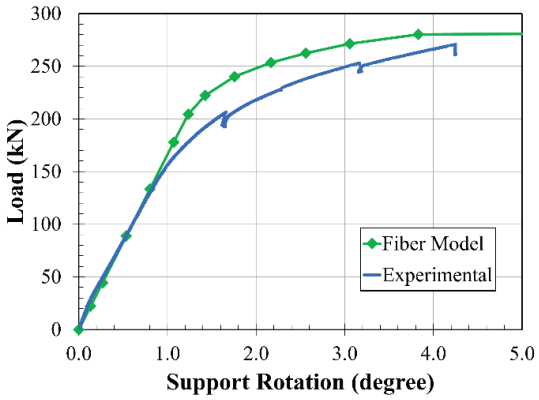

Figure 15: *Average experimental support rotation compared with fiber analysis results.*

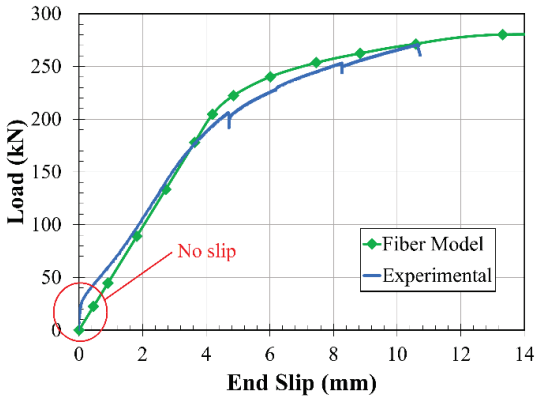

Figure 16: *Average steel-CLT slip at supports compared with fiber analysis results.*

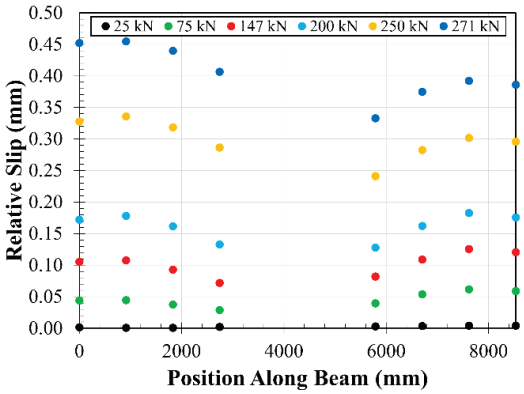

Figure 27: *Measured slip along the length of the beam measured from support-to-support.*

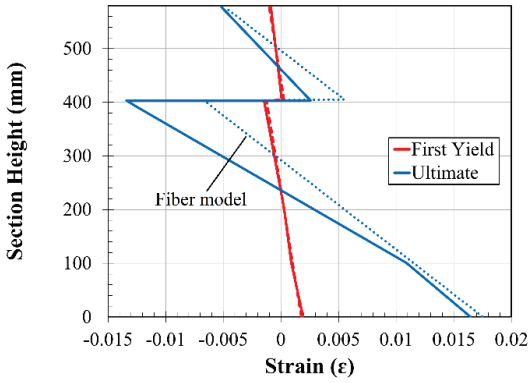

Figure 18: *Experimental yield and ultimate strain profiles compared with fiber analysis results (indicated by dashed lines).*

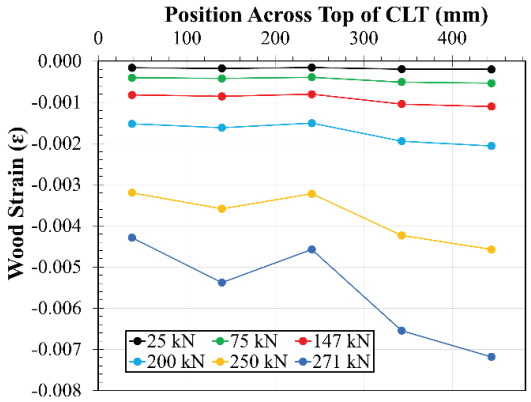

Figure 19: *Midspan strain distribution across the width on top of the CLT.*

Table 2: *Ultimate strength, average maximum rotation, average maximum slip, and relative stiffness.*

	Ultimate Strength (kN)	Support Rotation (degree)	End Slip (mm)	EI_{eff} (10^{12} Nmm^2)
Exp.	271	4.3	10.6	36.0
Fiber Anlys.	280	4.1	14.1	44.5
AISC	283	-	-	54.8

Table 3: *Yield and ultimate strength and midspan displacements.*

	Yield Load (kN)	Yield Disp. (mm)	Ult. Str. (kN)	Ult. Disp. (mm)
Exp.	147	49	271	254
Fiber Anlys.	200	58.7	280	241

4 DISCUSSION OF BEAM TEST RESULTS

The results demonstrate that the steel-CLT beam constructed with self-tapping screws exhibited partial-composite behavior based on the measured slip strain at the steel-CLT interface. However, prior to the initiation of slip, the beam exhibited near full-composite action as indicated by strain continuity at 25 kN shown in Figure 20. Using Equation (1), the composite action was determined to be 91.4% at 25 kN. After overcoming the initial friction provided by screw torquing, it is observed that the strain continuity at the interface was lost, and the slip strain increased with increasing loading as shown in Figure 21. Consequently, the composite action was calculated to be 46.0% and 37.9% at 75 kN and 147 kN, respectively. The increase in slip strain results from the relative slip between the steel and CLT, as pictured in Figure 22, since the self-tapping screws are deforming due to the shear flow occurring at the interface. Thus, it was observed that the composite action between the steel CLT reduces as the load-slip response increases.

The test also produced some notable results that are useful for design purposes. Firstly, it was observed that the CLT was under uniform compression across the width until reaching large displacements, suggesting that there was no major shear lag observed in the CLT deck. This means that the entire width of the CLT can be accounted for in the calculations. Additionally, it was observed that the CLT deck provided adequate support of the steel compression flange against lateral torsional buckling. Since this beam test configuration does not mimic a real floor system application where a much wider panel would typically be used, it is useful to know that the CLT can be relied upon to provide continuous bracing against lateral-torsional buckling even at a relatively narrow slab width.

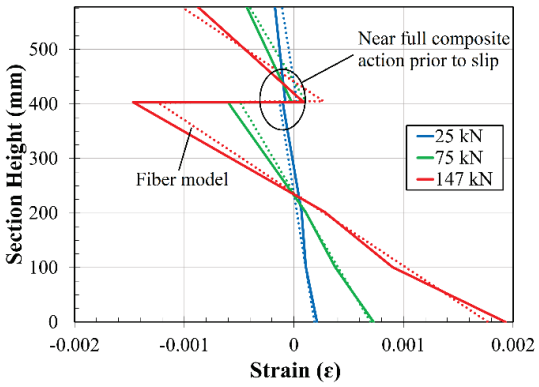

Figure 20: *Experimental service-level strain profile of section compared with fiber analysis results (indicated by dashed lines).*

https://doi.org/10.52202/069179-0439

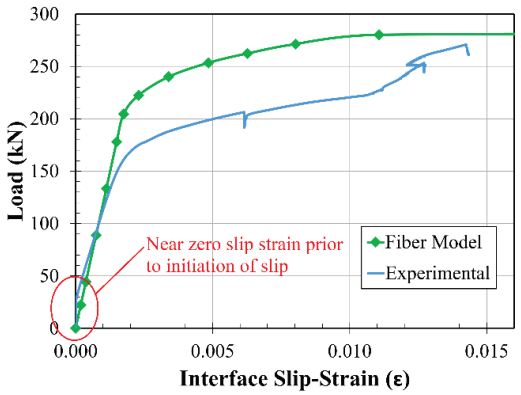

Figure 21: *Experimental slip strain at midspan between the steel flange and CLT slab*

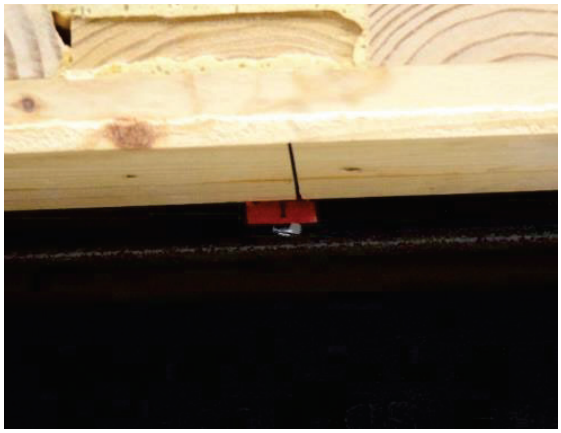

Figure 22: *Relative slip between the steel flange and CLT deck at support location*

Overall, the 2D fiber model predicted the beam behavior with reasonable accuracy compared to the experimental steel-CLT beam, considering the simplicity of the model and various underlying assumptions. From the fiber analysis, the percentage composite action at the steel-CLT interface was determined to be 41 percent at 111.2 kN. This percentage composite action was assumed constant throughout the fiber model analysis. The fiber analysis results yielded accurate ultimate strength, maximum rotation, and strain profiles through the section (Figures 20 and 21). Compared to the experimental steel-CLT behavior, the fiber analysis results predicted the ultimate strength to be 3% greater and the maximum rotation to be 5% lower. However, the fiber analysis results overestimated the maximum slip and initial stiffness by approximately 32% and 20%, respectively. Several limitations exist within the model due to assuming elastic-perfectly plastic behavior of the steel and CLT and assuming constant percentage composite action throughout the analysis.

Furthermore, the AISC calculations adapted from steel-concrete composite beam design predicted the ultimate capacity of the beam within 4 percent accuracy, but overestimated the initial stiffness by about 47 percent, as reported in Table 2 and Figure 23.

Finally, the experimentally obtained moment curvature response is provided in Figure 23 by taking the derivative of measured rotation at load points, and compared against AISC capacity and stiffness, fiber analysis, and 0% composite action (hybrid case). The experimental moment curvature is observed to closely align with the AISC stiffness until initiation of yielding. By accounting for the contribution of composite behavior, the flexural stiffness and moment capacity increased by nearly 40%, from the hybrid case.

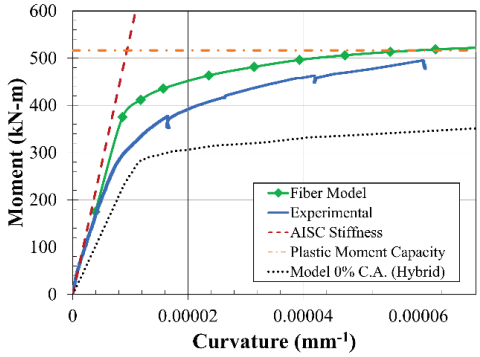

Figure 23: *Moment-curvature relationships for experimental steel-CLT beam and fiber model compared against AISC stiffness and plastic moment capacity.*

5 CONCLUSIONS

As demand increases for mass timber in high-rise construction, there exists a need for design guidance for efficient structural systems such as steel-CLT floor systems. A steel-CLT composite beam constructed with self-tapping wood screws was monotonically tested under a four-point bending setup and compared with analysis results obtained from a fiber model. Test results demonstrate almost full-composite (greater than 90%) behavior prior to connection slip but reducing to partial composite (about 40% prior to steel yielding) behavior with increasing load due to screw deformation. For design purposes, it was observed that the CLT deck was under near uniform compression and the deck provided continuous bracing for the steel against lateral torsional buckling. The fiber analysis model predicted the steel-CLT flexural response with reasonable accuracy, including the ultimate strength, maximum rotation, and strain profiles, but has limitations due to its assumptions and simplicity. Calculations adapted from steel-concrete composite design proved to be accurate for calculating the plastic moment capacity of the beam but overestimated its flexural stiffness.

6 FUTURE RESEARCH

Additional testing will be completed utilizing self-tapping screws in steel-CLT composite beams with the aim to develop a design guide for practicing engineers.

https://doi.org/10.52202/069179-0439

Parameters that will be investigated will include increasing CLT width, adjusting screw spacings, minor strength CLT bending (perpendicular orientation), and the contribution of concrete topping. Furthermore, the steel-CLT beams will be modelled in finite element analysis software to gain a deeper understanding of steel-timber flexural behavior.

ACKNOWLEDGEMENT

This research is financially supported by the United States Department of Agriculture (USDA) under the Wood Innovations Grant, 21-DG-11083150-150, with additional financial and in-kind support from the Softwood Lumber Board, American Institute of Steel Construction, SmartLam, and Simpson Strong-Tie.

REFERENCES

[1] A. Hassanieh, H. R. Valipour, and M. A. Bradford, "Experimental and numerical investigation of short-term behavior of CLT-steel composite beams," *Engineering Structures*, vol. 144, pp. 43–57, May 2017, doi: 10.1016/j.engstruct.2017.04.052.

[2] H. Merryday, K. Sener, and D. Roueche, "Pushout tests on steel-timber connections using self-tapping screws," presented at Structures Congress 2023, New Orleans, United States, May 2023.

[3] American Wood Council (AWC), *NDS-National Design Specification for Wood Construction,* Leesburg, VA., 2017.

[4] ASTM, *Standard Test Methods for Density and Specific Gravity (Relative Density) of Wood and Wood-Based Materials.* ASTM D2395-21. West Conshohocken, PA., 2021.

[5] ASTM, *Standard Test Method for Determining Bending Yield Moment of Nails.* ASTM F1575-21. West Conshohocken, PA, 2021

[6] ASTM, *Standard Test Methods for Single-Bolt Connections in Wood and Wood-Based Products.* ASTM D5652-21. West Conshohocken, PA., 2021.

[7] M. Potuzak, K. Sener, and D. Roueche,"Numerical studies on the flexural behavior of behavior of steel-timber composite floor systems," presented at Structures Congress 2023, New Orleans, United States, May 2023.

[8] American Institute of Steel Construction (AISC), *Steel Construction Manual, Fifteenth Edition*, Chicago, IL, 2017.

https://doi.org/10.52202/069179-0439